AAS 23-203

CONSTELLATION DESIGN TO SUPPORT CISLUNAR SURVEILLANCE LEVERAGING SIDEREAL RESONANT ORBITS

Maaninee Gupta[*], Kathleen C. Howell[†], and Carolin Frueh[‡]

There is a growing interest in trajectories to support missions throughout cislunar space, specifically the region beyond GEO and through the vicinity of the Moon and the L_1 and L_2 libration points. Multiple satellites, potentially in formations or constellations, assist with the monitoring and surveillance of cislunar space for long-term sustainable operations. This investigation explores resonant orbits and libration point orbits in sidereal resonance for hosting observer satellites that span cislunar space. Constellations of observers are designed, and options for various different observer orbits are explored. The efficacy of the constellations for surveillance applications is evaluated in both the CR3BP and ephemeris models.

With the anticipated increase in the number of missions to the lunar vicinity, surveillance in the Earth-Moon cone is warranted, but surveillance throughout the expanded cislunar region also offers advantages. While the provisions for surveillance and tracking are well established in the vicinity of the Earth, the existing architecture is not necessarily extendable throughout all cislunar space. The large volume of cislunar space renders a single satellite insufficient to adequately monitor the region. Specific neighborhoods within this larger space, including the regions near the L_1 and L_2 libration points, are of increasing interest as well. As such, specialized satellites near these regions to provide uninterrupted surveillance offer unique advantages. Thus, to sufficiently monitor cislunar space, as well as such specific regions of interest, it is necessary to design a constellation of satellites rather than a single vehicle. In tandem, these satellites are able to continuously observe objects in this large volume of space encompassing the lunar orbit.

While the vicinity of the L_2 libration point is identified as a region of interest, it is associated with additional challenges due to the communications "blind spot" behind the Moon. One approach, detailed by Farquhar,[1] utilizes relay satellites in halo orbits to establish uninterrupted two-way communications between the lunar far-side and the Earth. The Chinese Lunar Exploration Program, CLEP, applied the concept to facilitate communications between the Chang'e 4 lander, on the lunar far-side, and the Earth, via the Queqiao relay satellite based in an L_2 halo orbit.[2] In this investigation, the same principles are extended for applications focused upon cislunar space surveillance. Additionally, while the Deep Space Network (DSN) typically supports missions to cislunar space and beyond, it is routinely over-subscribed and congested.[3] The level of demand is only expected to increase with time as the number of missions returning to the lunar vicinity increases. Thus, to

[*]Ph.D. Student, School of Aeronautics and Astronautics, Purdue University, West Lafayette, IN 47907; gupta208@purdue.edu

[†]Hsu Lo Distinguished Professor of Aeronautics and Astronautics, School of Aeronautics and Astronautics, Purdue University, West Lafayette, IN 47907; howell@purdue.edu

[‡]Associate Professor, School of Aeronautics and Astronautics, Purdue University, West Lafayette, IN 47907; cfrueh@purdue.edu

mitigate the lack of lunar far-side communications and to alleviate the reliance on the DSN, a data relay satellite (DRS) is included in the trajectory design for any surveillance constellation in this investigation.

The present investigation extends the work by Frueh et al.[4,5] and Gupta et al.[6,7] in the exploration of cislunar surveillance for space domain awareness (SDA) applications. The complex gravitational environment of cislunar space necessitates the use of a multi-body dynamical model, incorporating the gravitational influences of the Earth and the Moon. The Earth-Moon Circular Restricted Three-Body Problem (CR3BP) is, thus, leveraged as the primary dynamical model for trajectory design. The CR3BP introduces a variety of periodic orbits that traverse extensively throughout cislunar space, as well as orbits that yield focused access to specific regions of interest. To enforce phasing between orbits, periodic orbits in sidereal resonance, such as resonant members of the libration point orbit families, are investigated. Earth-centered sidereal resonant orbits corresponding to different resonance ratios are also incorporated in a 'constellation' design due to their unique geometries and Earth-Moon access. As an example, various constellations comprised of as many as four satellites, including data relay satellites, are proposed. The design methodology, however, is applicable for more/fewer satellites as well. Beyond the CR3BP, the orbits in the satellite constellations are also validated in the Earth-Moon-Sun-Jupiter ephemeris model.

DYNAMICAL MODELS

This investigation leverages two dynamical models for the construction and analysis of the proposed orbits. The first model is the Circular Restricted Three-Body Problem (CR3BP), that is employed in the computation of relevant baseline orbits. Further analysis of the orbits in a higher-fidelity dynamical environment is then delivered via the N-body ephemeris model, incorporating the additional gravitational perturbations due to the Sun and Jupiter.

Circular Restricted Three-Body Problem

The CR3BP is an autonomous dynamical model that incorporates the gravitational influences of two planetary bodies, a planet-moon or a Sun-planet pair. The Earth and the Moon produce the greatest levels of acceleration on spacecraft traversing the cislunar region and, thus, these are the two bodies that comprise the model in this analysis.[4] The Earth and the Moon, termed the primaries and denoted as P_1 and P_2, respectively, are assumed to be point masses orbiting their mutual barycenter in circular orbits. The third body represents a smaller body of infinitesimal mass relative to the masses of the primaries and is denoted as P_3. The CR3BP allows the motion of the third body, the spacecraft, to be modeled under the gravitational influence of P_1 and P_2. A rotating frame based in the motion of the primaries is adopted to describe the behavior of the spacecraft governed by the two bodies. This rotating frame moves at a constant rate, $\dot{\theta}$, relative to an inertial frame, and this rate is equal to the mean motion of the system. Figure 1 represents the orientation of the rotating reference frame, denoted $\hat{x}$-$\hat{y}$-$\hat{z}$, relative to the inertial reference frame, denoted $\hat{X}$-$\hat{Y}$-$\hat{Z}$, with both frames centered on the system barycenter, B, where the vector bases are dextral, orthonormal triads. (Carets identify vectors of unit length.)

The quantities l^*, m^*, and t^*, termed the characteristic length, characteristic mass, and characteristic time, respectively, are introduced to nondimensionalize the equations of motion in the CR3BP. The characteristic length is equal to the constant distance between the primaries, the characteristic mass is equal to the sum of the masses of the primaries and, finally, the characteristic time is defined such that the nondimensional gravitational constant, $\tilde{G}$, is equal to unity. The nondimensional

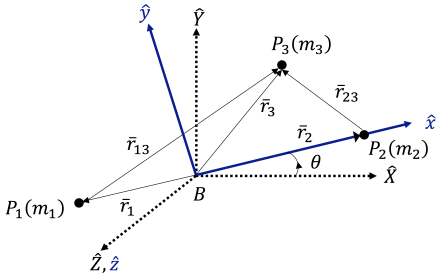

Figure 1. Schematic of the CR3BP inertial and rotating frames.

equations of motion that represent the motion of P_3 as expressed in the P_1-P_2 rotating frame are, thus, represented as,

$$\ddot{x} - 2\dot{y} = \frac{\partial U^*}{\partial x}, \quad \ddot{y} + 2\dot{x} = \frac{\partial U^*}{\partial y}, \quad \ddot{z} = \frac{\partial U^*}{\partial z} \tag{1}$$

The quantity U^* is the pseudo-potential function, expressed as,

$$U^* = \frac{1-\mu}{r_{13}} + \frac{\mu}{r_{23}} + \frac{x^2+y^2}{2} \tag{2}$$

where μ is the system mass parameter evaluated as $\mu = \frac{m_2}{m_1+m_2}$, and is roughly equal to 0.01215 for the Earth-Moon system. Additionally, r_{13} and r_{23} denote the nondimensional distances between the Earth and the spacecraft as well as the Moon and the spacecraft, respectively. The coordinates (x, y, z) correspond to the nondimensional position of the spacecraft relative to the system barycenter in the Earth-Moon rotating frame; similarly, $(\dot{x}, \dot{y}, \dot{z})$ represents the velocity components of the spacecraft as viewed in the rotating frame. Five equilibrium solutions that are termed the libration points or the Lagrange points exist in the CR3BP, denoted as L_i for $i = 1, ..., 5$. Although a closed-form solution does not exist for the equations of motion in the CR3BP, one integral of the motion aids numerical analyses. This quantity is termed the Jacobi constant and is evaluated in terms of the pseudo-potential function and the velocity magnitude for P_3 in the rotating frame, v, as $C = 2U^* - v^2$. Bounds on the allowable motion of P_3 at a given Jacobi constant value are indicated via three-dimensional Zero Velocity Surfaces (ZVSs) and planar Zero Velocity Curves (ZVCs) in configuration space. Regions that are inaccessible at given energy levels are termed the *forbidden regions*, and a change in velocity (energy) is necessary to access these regions.

N-Body Ephemeris Model

The N-body ephemeris model offers a higher level of fidelity than the CR3BP, allowing the addition of other celestial bodies that influence the motion of a spacecraft. Contrary to the formulation of the CR3BP, the ephemeris model is based in an inertial frame, centered on some central body denoted P_q. The spacecraft, denoted P_i, is assumed to move under the gravitational impact of this central body, as well as other influential celestial bodies, denoted P_j. As in the CR3BP, all bodies are modeled as point masses. The true locations of the bodies that comprise the N-body model, both relative to the spacecraft and to the central body, yield a more accurate representation of the dynamical motion of the spacecraft. The relevant equations of motion that govern the spacecraft

dynamics are second-order vector differential equations, i.e.,

$$\ddot{\bar{r}}_{qi} = -G\frac{(m_i + m_q)}{r_{qi}^3}\bar{r}_{qi} + G\sum_{\substack{j=1 \\ j\neq i,q}}^{N} m_j \left(\frac{\bar{r}_{ij}}{r_{ij}^3} - \frac{\bar{r}_{qj}}{r_{qj}^3}\right) \tag{3}$$

where $\bar{r}_{qi}$ represents the position of the spacecraft relative to the central body, $\bar{r}_{ij}$ denotes the position of each perturbing body with respect to the spacecraft, and $\bar{r}_{qj}$ locates the position of each perturbing body relative to the central body. The DE421 planetary ephemerides retrieved from the NASA Jet Propulsion Lab (JPL) Navigation and Ancillary Information Facility (NAIF) are utilized to obtain the relative positions and velocities of the various celestial bodies in this model.[8] In the context of modeling spacecraft motion in the cislunar dynamical environment, it is generally reasonable to select the Earth as the central body, with additional perturbing effects resulting from the inclusion of the Moon, the Sun, and Jupiter.

CR3BP PERIODIC ORBITS

Natural or ballistic propagation of trajectories in the CR3BP using the differential equations in Equation (1) does not necessarily yield periodic solutions. However, differential corrections schemes are effective to construct periodic orbits and, by extension, families of periodic orbits that are characterized by similar geometries and dynamical properties. In the Earth-Moon CR3BP, orbits are classified into Earth- or Moon-centered periodic orbits, libration point orbits in the vicinity of the libration points, and resonant orbits. Earth-centered orbits include the CR3BP analogs of Keplerian orbits, such as conics in LEO or GEO. Orbits centered on the Moon in the rotating frame, however, exhibit more complex motion that depart from traditional Keplerian geometries. Examples of such orbits include, but are not limited to, the distant prograde orbits (DPOs), distant retrograde orbits (DROs), period-multiplying DROs, and the H_1 and H_2 families of prograde orbits.[9] Libration point orbits (LPOs) also exist in the vicinity of all libration points in the rotating frame. However, due to their proximity to the Moon and, thus, their applicability for surveillance missions, LPOs near the L_1 and L_2 libration points are a particular focus. Examples of LPO families include the planar Lyapunov orbits and the spatial northern and southern halo orbits. Sample L_1 and L_2 Lyapunov orbits are plotted in Figure 2(a) as viewed in the Earth-Moon rotating frame. Examples of Moon-centered orbits with unique geometries in the rotating frame appear in Figure 2(a) as well, with a distant prograde orbit plotted in gold, and orbits from the H_1 and H_2 orbit families plotted in light blue and light green, respectively. Considering the proximity of these orbits to the Moon as well as the L_1 and L_2 libration points, spacecraft in orbits from these families can aid surveillance further from the Earth.

While the LPOs and Moon-centered orbits provide localized cislunar access, sidereal resonant orbits possess expansive geometries that sweep through broader areas of the Earth-Moon neighborhood. Such orbits possess periods that are commensurate with the lunar sidereal period, and are characterized by their resonance ratio, denoted p:q, that is a simple integer ratio of the orbital period of the Moon and the spacecraft orbit. A spacecraft in a p:q resonance with the Moon encircles the Earth p times in the interval required for the Moon to complete q revolutions of the Earth. For resonant orbits computed in the Earth-Moon CR3BP, the ratio of the orbital periods is not a perfect integer, i.e., the spacecraft completes p orbits in approximately the time that the Moon completes q revolutions of the Earth. Resonance ratios with $p > q$ are indicative of interior resonances, while ratios with $p < q$ describe exterior resonances. Additionally, since periodic orbits in the CR3BP

exist as families of solutions that share similar characteristics, such is also true of resonant orbits. One methodology for the construction of a resonant orbit in the CR3BP relies on first computing its two-body model counterpart.[10] Since the CR3BP incorporates the gravitational influence of the Moon on the spacecraft, simply propagating the two-body orbit using the CR3BP equations of motion is not sufficient, and the initial conditions for the orbit require adjustment via differential corrections to produce a closed periodic resonant orbit. Generally, resonant orbits computed using this methodology retain the geometries of their Keplerian counterparts, specifically near the vicinity of the Moon. However, it is also possible to produce resonant orbits that exhibit a departure from their characteristic two-body resonant geometries near the vicinity of the Moon while retaining their near-resonant orbit periods. A grid search methodology, adapted from Anderson et al., is implemented to directly compute these CR3BP resonant orbits with more complex geometries near the lunar vicinity.[11] Specifically, a fixed-time single shooting algorithm is implemented in search of perpendicular crossings on the $\hat{x}$-axis and with propagation times that are commensurate with the lunar sidereal period or a suitable multiple. Due to their proximity to the Moon, orbits constructed via this methodology generally tend to be unstable in a linear sense. Resonant orbits corresponding to various resonance ratios that are produced via either of these two methodologies are plotted in Figure 2(b). The orbits that appear in the figure belong to families that possess similar geometries but evolve through other energy levels. Notably, for cislunar surveillance applications, resonant orbits provide options for orbits that pass close to the Earth and the Moon, while also sweeping through the vicinity of the libration points.

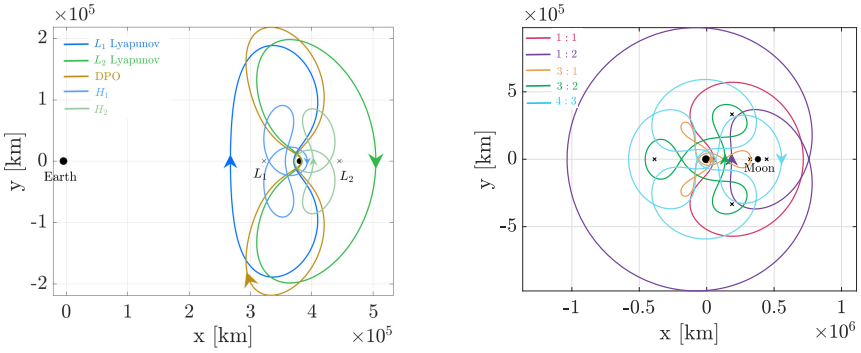

(a) LPOs and Moon-centered orbits.

(b) Resonant orbits.

Figure 2. Periodic orbits computed in the Earth-Moon CR3BP plotted in the Earth-Moon rotating frame. Arrows indicate the direction of motion along the orbits.

OPTIONS FOR SURVEILLANCE ORBITS

The CR3BP supplies an extensive number of periodic orbits spanning various energies and geometries, some included here. Individually, CR3BP periodic orbits can yield localized access for focused cislunar surveillance. For instance, in addition to observations toward the Earth, L_1 libration point orbits are applicable for monitoring the near-side of the Moon; L_2 libration point orbits, then, are useful for surveying the lunar far-side. Broader access of cislunar space, such as the volume of space near the Earth but beyond GEO, as well as the L_3 libration point, is more broadly achievable by leveraging resonant orbits that traverse larger areas. Combinations of satellites, or space-based *observers*, in various orbits together provide constant surveillance of cislunar space, with monitoring capabilities for specific regions of interest as well. Such a constellation of observers may operate in unique orbits that span the volume of cislunar space to provide comprehensive coverage.

Various sidereal resonant orbits are incorporated into the constellation design due to their expansive geometries. Additionally, when available, LPOs and Moon-centered periodic orbits possessing periods that are resonant with the lunar orbit period are also examined. The resonance between the orbits and the Moon and, by design, other observers in the constellation, ensures that the relative phasing of the spacecraft in the constellation is naturally maintained.

Orbits for Data Relay Satellites

To conduct and maintain cislunar Space Domain Awareness (SDA) operations, it is necessary to facilitate periodic communications and data relay between the space-based observers and the Earth. However, the large volume of cislunar space that requires surveillance and, consequently, the long distances between observers in the lunar vicinity and the Earth, introduces challenges to sustain constant ground-based communications. These concerns are alleviated by potentially incorporating a Data Relay Satellite (DRS) into the surveillance constellation architecture. The wide variety of geometries available in CR3BP periodic orbits allows the selection of a DRS orbit such that it periodically interfaces with observers in specific cislunar regions of interest, such as the libration points, while also passing close to the Earth. Thus, when direct communications with the Earth are not possible, but an exchange is necessary, data from the observers may be relayed to the Earth by means of the DRS. Favorable characteristics of periodic orbits suitable for the DRS include short periods, repeated and close encounters with both the Earth and the Moon, and the orbital stability to sustain long-term operations as well. Operational stability is quantified via the periodic orbit stability index, that is a function of the eigenvalues of the monodromy matrix associated with the orbit.[6,12] Additionally, the DRS must be phased such that it encounters the observers in their orbits periodically as well, ideally without the necessity of phasing maneuvers. Given these characteristics, sidereal resonant orbits, such as those introduced in Figure 2(b), offer viable options for hosting a cislunar DRS.

One example of orbits that facilitate cislunar surveillance and data relay from the observer satellites to the Earth is the family of prograde orbits in 2:1 sidereal resonance with the Moon. A subset of the orbit family, as viewed in the Earth-Moon rotating frame, appears in Figure 3(a) with orbits colored by their respective Jacobi constant values. Orbits in this family provide repeating Earth-Moon transfer opportunities and complete approximately two revolutions of the Earth during every lunar sidereal period. This fact is evident by visualizing the motion in an Earth-centered inertial frame, as demonstrated in Figure 3(b), where each *elliptical lobe* corresponds to a time-of-flight of approximately half the lunar sidereal period. In the inertial frame view, the inertial precession of the orbits possessing lower Jacobi constant values as a result of the lunar encounter is also apparent. A specific orbit from this family that passes the Earth at the radius of a geosynchronous orbit, while simultaneously traveling within $10,000\ km$ of the lunar surface, was previously identified.[7] This particular orbit is described with a Jacobi constant value of 2.5946, and a period approximately equal to the lunar sidereal period, $28.13\ days$. However, noting the shift in the periapse and perilune radii of orbits in Figure 3(a) as a function of the Jacobi constant value across the family, a multitude of orbits with various perigee and perilune values are also available. The evolution of the stability index and the orbit period as a function of the Jacobi constant value along the subset of this orbit family is plotted in Figure 3(c). Notably, while they are not in a precise sidereal resonance with the Moon, the orbits are closed and repeating in the rotating frame. Spacecraft in these orbits encounter the Moon once a month, while also traveling close to the Earth bimonthly. Despite the approximate sidereal resonance, this characteristic repeats over longer propagation times, offering convenient opportunities for natural ballistic access between the Earth and the Moon. In the inertial

frame, for longer propagation times, the location of the lunar encounter shifts to accommodate the longer orbit periods. As an example, an orbit from this family is propagated for 34 revolutions (approximately 956 $days$), and the resulting trajectory completely maps out the Earth-Moon planar subspace, as apparent in Figure 3(d). Despite the inertial precession of the perilune, the perigee altitude is maintained over successive revolutions. Thus, a data relay satellite in such an orbit repeatedly encounters the neighborhood of the L_1 and L_2 libration points as well as the Moon, that may be useful for transferring data from observers in such orbits back and to the Earth. Thus, in addition to yielding cislunar coverage for surveillance, the 2:1 resonance family provides options for orbits that yield opportunities for periodic data relay between the Earth and the observer satellites that comprise the surveillance constellation.

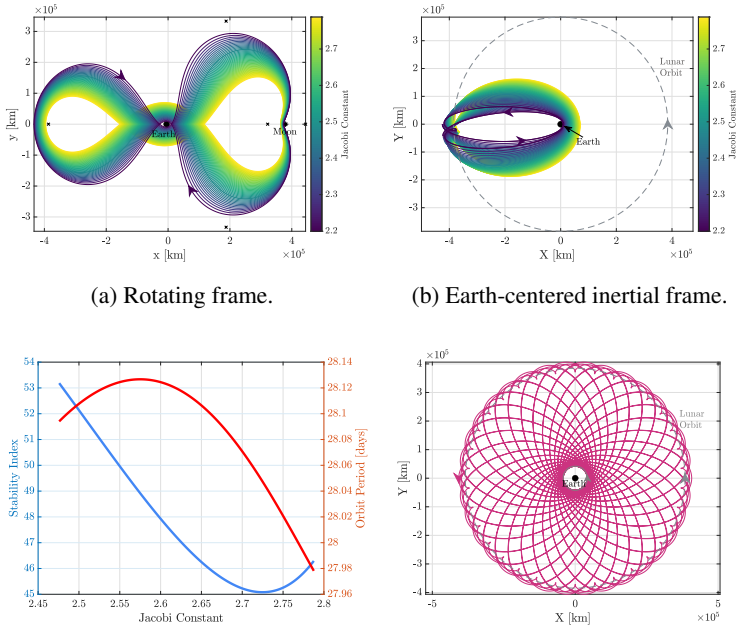

(a) Rotating frame.

(b) Earth-centered inertial frame.

(c) Stability index and orbit period.

(d) Long propagation of a sample orbit.

Figure 3. The CR3BP 2:1 sidereal resonant orbit family plotted in the Earth-Moon rotating and ECI frames. Also plotted are the orbit period, stability index, and long-term propagation of a sample 2:1 orbit viewed in the ECI frame.

Orbits for Space-Based Observers

While the selection of the DRS orbit supplies global coverage of cislunar space, a focus on the specific regions of interest within the entire volume of space is critical to facilitate surveillance.[13] As such, periodic orbits that yield coverage near the lunar vicinity are necessary. Specifically, the volume within a 30° cone with its vertex at the Earth facing out towards the Moon is identified as a high priority zone for maturing the current tracking and surveillance capabilities.[14,15] Periodic orbits near the L_1 and L_2 libration points offer options that remain in the lunar vicinity and inside the 30° "surveillance cone". However, as previously noted, spacecraft in orbits near the L_2 point do not establish a direct line-of-sight for communications with the Earth. Nevertheless, by incorporating the DRS into a surveillance constellation, these challenges are potentially mitigated. Various CR3BP periodic orbits are introduced and examined as potential hosts for observer satellites with on-board sensors that collect surveillance data.

A wide varied of geometries are available in multi-body periodic orbit families. Subsets from the families of L_1 and L_2 Lyapunov orbits, as well as distant prograde orbits (DPOs), are plotted in Figure 4. To interface with other vehicles in a constellation and maintain a relative phasing, specific orbits in a sidereal resonance with the lunar orbit are noted. Orbits in 1:1, 4:3, 3:2, and 2:1 resonance are available and are highlighted in black in the three orbit families. Awareness of for the energy levels at which these orbits exist allows potential transfer opportunities that minimize their relative velocities. While additional options for Moon-centered periodic orbits exist, of particular interest is a subset of the family denoted as the Period-3 Distant Retrograde Orbits (P3DROs) plotted in Figure 4(d). This orbit family bifurcates from the planar distant retrograde orbit family.[12] The periods of the orbits in Figure 4(d) span the range between 20.09 $days$ and 29.63 $days$, providing options for 1:1 sidereal resonant members. The family of P3DROs expands further to longer periods as well, but only the subset in the figure is examined due to their applicability to surveillance applications. An observer in such an orbit naturally passes back and forth between the lunar near- and far-sides, while remaining bounded to the illustrated orbit geometry.

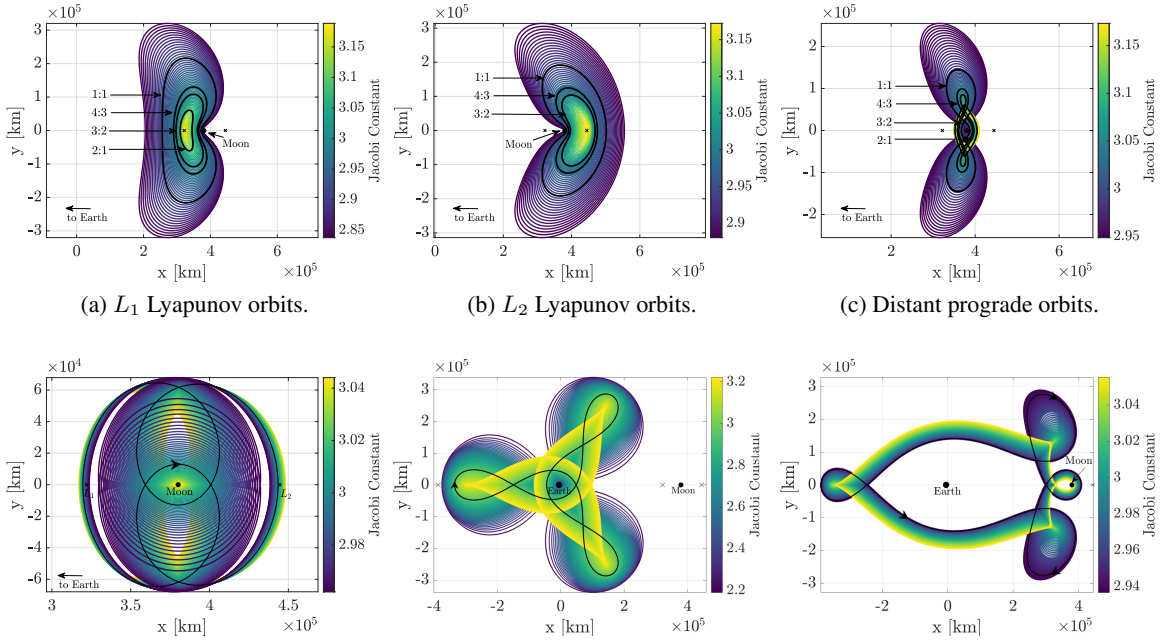

(a) L_1 Lyapunov orbits. (b) L_2 Lyapunov orbits. (c) Distant prograde orbits.

(d) Period-3 distant retrograde orbits. (e) 3:1 resonant orbits. (f) 4:3 resonant orbits.

Figure 4. Periodic orbits with various geometries for space-based sensor placement computed in the Earth-Moon CR3BP and plotted in the Earth-Moon rotating frame.

Resonant orbits characterized by other resonance ratios are also noted due to their footprint throughout cislunar space. Interior resonant orbits with shorter periods remain interior to the Earth-Moon system and typically pass close nearby to either the Earth or the Moon, or both. Such a feature is particularly useful for surveillance capabilities inside the 30° cone from the Earth to the Moon, within which ground-based space domain awareness capabilities are limited. Thus, space-based sensors in these resonant orbits facilitate the tracking of natural objects and assets in cislunar space. Some examples of interior resonant orbits that are suitable for Earth-Moon surveillance include, but are not limited to, members from the families of 3:1 and 4:3 resonances, constructed and plotted in the Earth-Moon rotating frame in Figure 4. In each family, orbits in black highlight the unique geometries of the orbit families and indicate the direction of motion along the orbits. In addition

to offering cislunar coverage, these orbits also encounter prograde 2:1 resonant orbits with every revolution, thus allowing inter-satellite communications and potential periodic data relay.

SAMPLE CONSTELLATION DESIGN

While the selection of some combination of orbits in a cislunar constellation is mission specific, an example of the selection process is detailed within the context of cislunar surveillance. A sample surveillance design is introduced and analyzed here, but the methodology is adaptable as necessary. Trajectories are selected for a four-satellite constellation; one of the four is a data relay satellite that periodically approaches the Earth near the GEO belt. The DRS is assumed to be operating in a 2:1 resonant orbit selected from the orbit family in Figure 3. The remaining three satellites, i.e., the observers, are distributed across cislunar space for a wide-ranging but also localized set of surveillance requirements. Specifically, a 3:1 resonant orbit, and two 1:1 sidereal resonant members from the L_1 and L_2 Lyapunov orbit families are selected as a sample constellation. Table 1 lists the Jacobi constant values and the orbital periods for the selected orbits, all plotted in Figure 5(a) as viewed in the Earth-Moon rotating frame. The 2:1 data relay satellite orbit is plotted in black, with the radius of a geosynchronous orbit indicated in blue. While this particular orbit is not precisely tangent to the GEO altitude, it passes the GEO belt fairly closely in the prograde direction. Notably, the 2:1 orbit periodically approaches the vicinity of the other observers, thus, allowing recurring opportunities for data relay away from the Earth. The selected 3:1 resonant orbit, plotted in purple, is defined with a higher Jacobi constant value than the other observers and, thus, exists at a lower energy level. Clearly, the perigee of this orbit is similar to the perigee radius for the prograde 2:1 resonant orbit. The observer in this 3:1 orbit completes three Earth revolutions in one month. The remaining two observers are assumed to operate in approximate 1:1 sidereal resonant L_1 and L_2 Lyapunov orbits that are plotted in blue and green, respectively. While the low amplitude of the L_2 Lyapunov orbit inhibits line-of-sight communications with the Earth, the selected data relay satellite passes sufficiently close to the orbit to relay data back to the Earth from the lunar far-side.

Table 1. Characteristics of the selected constellation orbits.

	Orbit	Jacobi Constant	Period [days]	Perilune Altitude [km]
DRS	2:1 Resonance	2.7029	28.07	11,268.53
Observer 1	3:1 Resonance	3.1302	28.07	65,343.97
Observer 2	1:1 L_1 Lyapunov	2.9148	28.07	5551.87
Observer 3	1:1 L_2 Lyapunov	2.9350	28.07	2258.36

A number of criteria are employed to evaluate the applicability and feasibility of the selected observer orbits for surveillance applications. First, for observers to obtain valuable surveillance data, the time within the surveillance cone by the observers is evaluated. Next, to minimize the reliance on direct communications with the Earth, the ability of the observers in their orbits to interface with the relay satellite in its orbit is examined. This metric is assessed in terms of line-of-sight access between the two spacecraft as well as the relative distance between the spacecraft over time. For spacecraft that are within $120,000\ km$ of each other at a given time, it is assumed that inter-satellite communications allow the relay of surveillance data from the observer to the DRS to occur. Naturally, the spacecraft on-board hardware drives the inter-satellite communications capabilities; however, this distance is assumed to be the nominal value for this investigation and may be modified as necessary. Based on this maximal range for communications, the relative phasing between

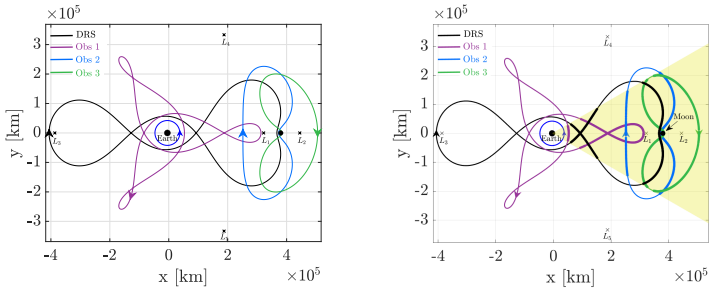

(a) Constellation orbits. (b) Surveillance cone.

Figure 5. Selected orbits for a set of satellites in a constellation as viewed in the Earth-Moon rotating frame and computed in the Earth-Moon CR3BP.

the DRS and the observers is determined as well. Contour maps are generated that aid preliminary selection of the relative phase to maximize the time within this communications range without the necessity for maneuvers. Finally, the velocities of spacecraft in such orbits are assessed to evaluate the relative speeds and relay times with respect to other orbits that comprise the constellation. The process of evaluating the feasibility of observer orbits is then demonstrated for the orbits described in Table 1.

Observers within the Surveillance Cone

To gauge the ability of the spacecraft in the observer orbit to track objects within the specialized region of interest, i.e., the surveillance cone, the total time spent within the cone for each orbit is evaluated. For the constellation as a whole, the goal is defined as at least one observer collecting surveillance data from inside the surveillance cone at all times.[14,15] The 30° surveillance cone is illustrated in Figure 5(b), with its vertex at the Earth and axis of symmetry directed toward the Moon, as viewed in the rotating frame. The constellation orbits occasionally pass in and out of the cone, with at least one observer inside the cone at all times. The locations along each orbit that fall within the surveillance cone are indicated by the bold trajectory arcs. Over the course of $28.07\ days$, the DRS in the 2:1 resonant orbit remains inside the cone for $9.32\ days$, or about 33% of its orbital period. However, the observer orbits remain within the cone for $9.33,\ 17.32$, and $25.84\ days$ for the 3:1, L_1 Lyapunov, and L_2 Lyapunov orbits, respectively. These times correspond to approximately $33\%,\ 61\%$, and 92% of the propagation times. Thus, over intervals when ground-based space domain awareness from the Earth is lacking, the observers are able to track and survey objects and activity near the Moon. It is also noted from Figure 5(b) that this particular 1:1 L_2 Lyapunov orbit remains almost entirely inside the surveillance cone, offering constant monitoring capabilities from the lunar far-side.

Line-of-Sight with DRS for Communications

Since the observers rely on the DRS for contact with the Earth when direct communications are unavailable, line-of-sight with the DRS in its orbit must be maintained. In the Earth-Moon CR3BP, line-of-sight between two spacecraft in their respective orbits may not be possible when occulted by either the Earth or the Moon. The constraint is, thus, formulated as,

$$acos\left(\frac{\bar{r}_{DRS-P_i}\cdot\bar{r}_{DRS-obs}}{||\bar{r}_{DRS-P_i}||\ ||\bar{r}_{DRS-obs}||}\right)\leq atan\left(\frac{R_{P_i}}{||\bar{r}_{DRS}-\bar{r}_{P_i}||}\right) \tag{4}$$

for $i = 1, 2$, corresponding to the Earth and the Moon, respectively. When Equation (4) is satisfied for either or both of the primaries, there exists no line-of-sight between the DRS and the observer satellite and, consequently, communications or data relay is not possible. Thus, within the scope of the current constellation architecture, observer orbits that enable line-of-sight with the DRS orbit are the focus. The line-of-sight constraint is enforced to maintain the path outside any eclipse by the Earth and the Moon and the results are plotted in Figure 6 for the orbits from Table 1. The operating orbit for the DRS, a prograde 2:1 resonant orbit, is plotted in black, and the three resonant observers are plotted in purple, blue, and green in Figure 6(a), Figure 6(b), and Figure 6(c), respectively. The red markers along each orbit identify the locations at which there exists no line-of-sight between the DRS and the observer. For the 3:1 resonant orbit observer, the Earth prohibits line-of-sight with the relay satellite for a total of $0.32\ days$ or $7.6\ hrs$ over the course of $28.07\ days$. For the observer in the L_1 Lyapunov orbit, the total time over which the constraint is violated is approximately $0.35\ days$ or $8.5\ hrs$, spread out over three separate intervals during one sidereal month. For the L_2 Lyapunov orbit in Figure 6(c), the lack of a line-of-sight and, thus, lack of data relay opportunities, occurs for a longer total duration: $0.6\ days$ or $14.5\ hrs$ over three intervals due to the Earth and two intervals due to the Moon. However and, in most part due to the geometry of the 2:1 resonant orbit, the communications link for all the observers with respect to the DRS persists for the majority of the trajectory.

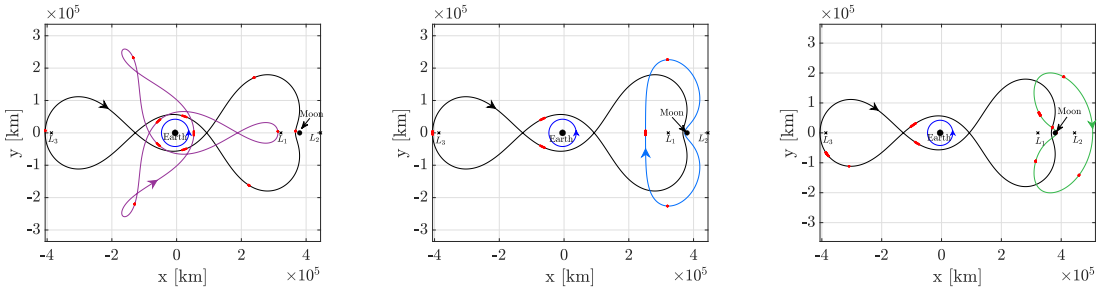

(a) 3:1 resonant observer. (b) L_1 Lyapunov observer. (c) L_2 Lyapunov observer.

Figure 6. Line-of-sight constraint for the DRS orbit and various observers. Red markers indicate locations of no line-of-sight between the DRS and the observer.

Distance Relative to the Data Relay Satellite

For data relay from the observer satellites to the DRS in the 2:1 resonant orbit, the distance of each observer relative to the relay satellite is also examined. As an example, and without any knowledge of the on-board hardware capabilities, it is assumed that when the observers are within $120,000\ km$ of the relay satellite, inter-satellite communications are possible. The total time that each observer is within communications range, relative to the relay satellite, serves as a metric to evaluate the efficacy of the observer orbits. Consider the isochronous distance for the second observer, i.e., the observer in the 1:1 L_1 Lyapunov orbit, relative to the DRS in its 2:1 resonant orbit. As a preliminary guess, the DRS is assumed to be located at apolune and the observer at perilune at $t = 0$. The initial conditions at those states for both orbits are propagated forwards in time using the CR3BP equations of motion for approximately one sidereal period. The isochronous relative distance and velocity between the two spacecraft is then evaluated. The data relay time is calculated, that is simply the total time that the observer is within the selected nominal range relative to the DRS (equal to $120,000\ km$ for this investigation).

For the sample scenario of a DRS and one observer in the L_1 Lyapunov orbit, assume a specific phasing. With the DRS initially at apolune (near L_3), and the Lyapunov orbit observer at perilune at $t = 0$, the resulting propagations appear in Figure 7(a). The relative distance between the two spacecraft is computed over the propagation time, that is one month. In Figure 7(b), the resulting distance is plotted as a function of time; the black line indicates the range limit below which data relay is assumed to be possible between the spacecraft. Clearly, despite the proximity of the orbits in configuration space, the initial relative phasing causes the spacecraft to deviate in phase from each other downstream. As such, the observer is outside the allowable data relay range for the majority of the propagation time, i.e., for a total of $27.73\ days$ of the $28.07\ day$ propagation time. The instances within the range are indicated by the bold arcs in each plot in Figure 7. For reference, the relative velocity between the two spacecraft is assessed as well and appears in Figure 7(c). For the times when the observer is within range of the DRS, its velocity relative to the DRS is excessively high, approaching almost $1.75\ km/s$, thus, data transmission is inhibited. Thus, the preliminary guess for the relative phasing between the DRS and the observer (apolune and perilune, respectively) is not feasible, and other strategies to determine more suitable phasing options are sought.

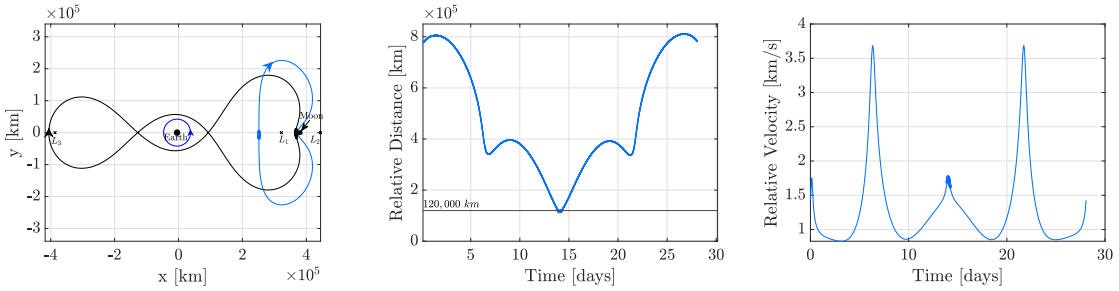

(a) Rotating frame. (b) Relative distance. (c) Relative Velocity.

Figure 7. DRS and an observer in the L_1 Lyapunov orbit propagated from apolune and perilune, respectively. The isochronous distance and the relative velocity between the two spacecraft is also plotted.

An angular representation for the locations along the DRS and the observer orbits is necessary to determine the ideal relative phasing between the two spacecraft. However, in contrast to Keplerian orbits, locations along CR3BP periodic orbits cannot be directly represented by angles, e.g., the true anomaly, mean anomaly, or eccentric anomaly, due to their complex geometries. This challenge is especially significant when working with resonant orbits due to their repeating geometries. For example, in the inertial frame, the 3:1 resonant orbit traces out three "elliptical-type revolutions" about the Earth. A cyclic metric that represents the passage of time along the orbit allows the relative phasing between orbits to be assessed. The trigonometric encoding methodology detailed by Lafarge et al. is adopted to discretize the orbit into angular locations.[16] This angle, termed the encoding angle, is evaluated as,

$$\xi = \frac{t_{po} \cdot 2\pi}{\mathbf{P}} \tag{5}$$

where $\mathbf{P}$ is the period of the orbit, and t_{po} is the time since a fixed reference state along the orbit ($t_{po} \in [0, \mathbf{P}]$). The selection of the fixed reference state along the orbit is arbitrary, and is assigned to be apolune in this investigation. Thus, $\xi = 0$ corresponds to apolune, and $\xi = \pi$ corresponds to the half-period location along the orbit. Specific locations along the orbits for the data relay satellite and the observers are discretized and represented by their respective encoding angles.

Returning to the feasibility of the 1:1 sidereal L_1 Lyapunov orbit for the selected prograde 2:1 resonant orbit, the locations along the orbits represented by their encoding angles are plotted in Figure 8. For each ξ_{DRS} and ξ_{obs} encoded angle along both orbits as appearing in Figure 8, the corresponding states are propagated for one sidereal period. A contour plot identifying the time that the spacecraft are within relay range (distance $\leq 120,000\ km$) over the course of one month is generated for each encoding angle combination. The resulting map appears in Figure 9(a). Previously, the preliminary guess for the phasing between the 2:1 resonant orbit for the DRS and the L_1 Lyapunov orbit for the observer is assumed as an initial phase represented by $\xi_{DRS} = 0\ [rad]$ and $\xi_{obs} = \pi\ [rad]$, that yields only $0.33\ days$ of relay time over one month. However, Figure 9(a) reveals options for relative phasings that result in significantly longer data relay times, up to $8\ days$ over one sidereal period. The locations at which the spacecraft are within communications range are denoted by the bold arcs in Figure 9(b), and the red markers locate the initial locations of the DRS and the observer in their respective orbits. The CR3BP trajectories propagated over five months corresponding to both the DRS and the observer, appear in Figure 9(c) as plotted in an Earth-centered inertial view. As the DRS in its 2:1 orbit, in black, precesses in the inertial frame to maintain its resonance with the Moon, the 1:1 Lyapunov orbit follows over subsequent revolutions. Since the orbital periods are all in equal resonance with the Moon and, as a result, with each other, the feasible phasing over one month persists over time as well. Consequently, the relative distance between the L_1 observer and the DRS is consistent over five months, as apparent in Figure 9(d). The two spacecraft maintain their relative phase as determined from the contour plot, and the relay time as evaluated over one month persists through longer propagation times as well. For a five month propagation time, a total of $42.02\ days$ of relay opportunities exist between the observer and the DRS. This value corresponds to approximately 30% of the propagation time, a significant difference from the preliminary guess that yields relay opportunities for only approximately 1.2% of the propagation time. Additionally, while the total relay time is the primary criterion in this investigation, this methodology is adaptable for the determination of the relative phase to accommodate other desired metrics as well. The same process is repeated for the other observers in the constellation. Rather than guessing and checking, angle encoding and contour plots are leveraged to determine the phase difference between the DRS and each observer such that the time within a specified communications range is maximized.

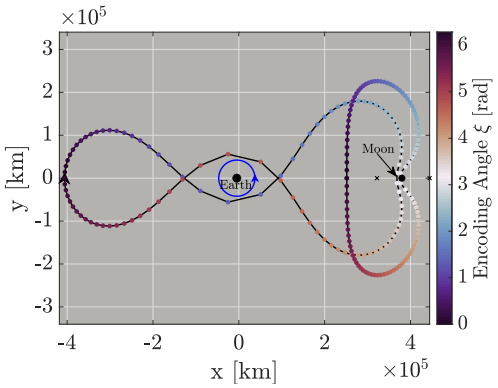

Figure 8. Trigonometric encoding for the DRS and the Lyapunov orbits.

To demonstrate the adaptability of the methodology, shift to an observer in a 3:1 resonant orbit. The appropriate contour plot appears in Figure 10. The ideal phase that maximizes relay time corresponds to $\Delta\xi = \pi\ [rad]$, yielding $3.5\ days$ of relay opportunities per revolution, and is propagated for five sidereal periods. The locations at which data relay windows occur are indicated in Figure 10(b) as viewed in the rotating frame, with the red markers locating the initial position of each spacecraft. Another notable feature of this particular resonant orbit, in addition to its proximity to the lunar vicinity, is repeatable passes to the vicinity of the GEO belt, as plotted in blue in

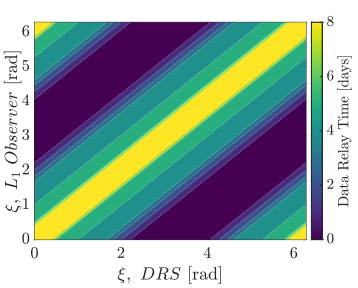

(a) Contour plot for total relay time.

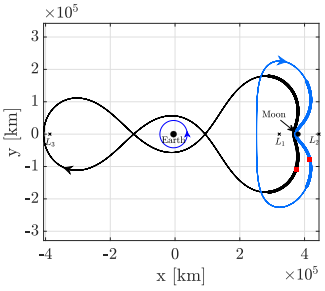

(b) Relay locations, rotating frame.

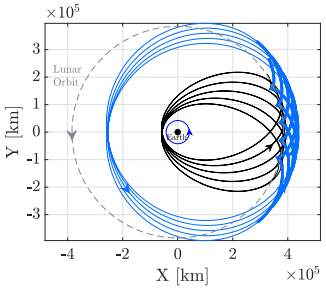

(c) Relay locations, inertial frame.

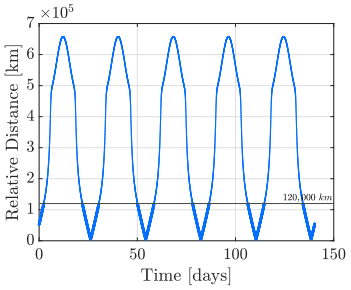

(d) Relative distance.

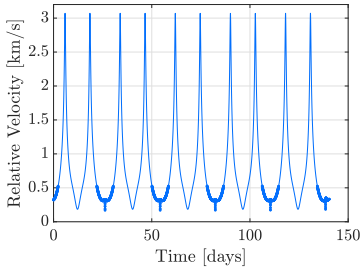

(e) Relative velocity.

Figure 9. Contour plot for relative phasing and data relay times for the observer in the 1:1 L_1 Lyapunov orbit. Relay opportunities are highlighted in bold along the orbits. Also plotted are the distance and velocity of the observer relative to the DRS.

Figure 10(b) and in the inertial frame in Figure 10(c). Thus, while the total time for data relay to the relay satellite in the 2:1 resonant orbit may be limited, as identified by the contour plot, the observer spacecraft in this orbit is able to communicate directly with the Earth as well. Over five months, because of their periods, the phasing with the DRS is maintained without a requirement for maneuvers. Such is apparent in Figure 10(d), where the relay opportunities repeat every month. A similar analysis for the 1:1 L_2 Lyapunov orbit reveals the ideal phasing for data relay to the DRS orbit as well, as demonstrated in Figure 11. The ideal phasing predicted by the contour plot in Figure 11, resulting in over 4.5 $days$ of relay time, is non-intuitive for this particular orbit. The locations at which the observer is within range of the DRS, indicated by the bold markers in Figure 11(b) and Figure 11(c), occur as the DRS is departing the lunar vicinity and enroute to the vicinity of the Earth. Thus, the observer is able to transfer surveillance data from the lunar far-side to the DRS for further relay to the Earth. For this orbit as well, the relative phasing for the two spacecraft persists over subsequent revolutions, and the observer is within $120,000$ km of the DRS for 24.3 $days$ over five months, as apparent in Figure 11(d). In addition to the relay opportunities when the observers are within the nominal communications range of the DRS, each observer maintains line-of-sight with the DRS for over 95% of the propagation time. Also, besides the observer in the L_2 Lyapunov orbit, the orbits themselves possess geometries such that direct communications with the Earth are possible as well.

Velocity Relative to the Data Relay Satellite

While the line-of-sight and range considerations for data relay are critical, it is also useful to compare the velocities of the observers relative to the DRS. The relative velocity metric is especially

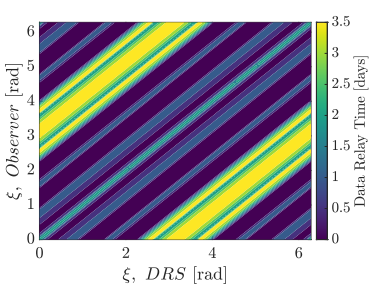

(a) Contour plot for total relay time.

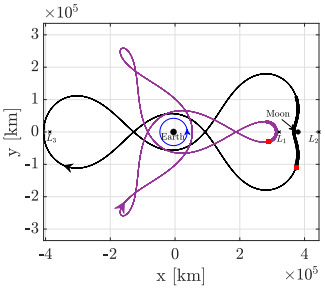

(b) Relay locations, rotating frame.

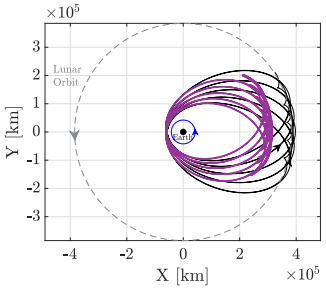

(c) Relay locations, inertial.

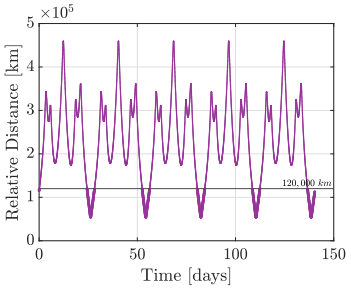

(d) Relative distance.

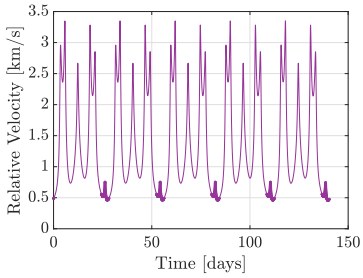

(e) Relative velocity.

Figure 10. Contour plot for total relay time for the observer in the 3:1 resonant orbit. Data relay locations are highlighted in the Earth-Moon rotating frame.

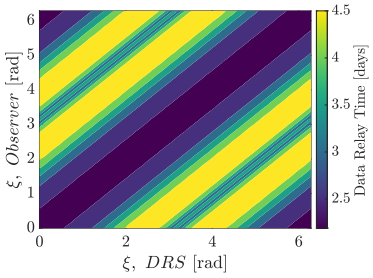

(a) Contour plot for total relay time.

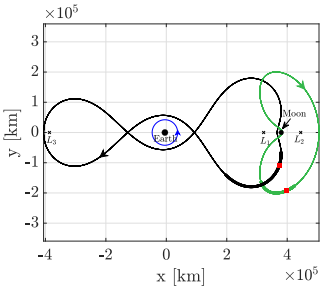

(b) Relay locations, rotating frame.

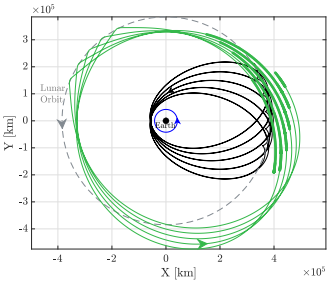

(c) Relay locations, inertial frame.

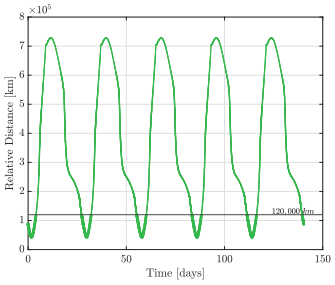

(d) Relative distance.

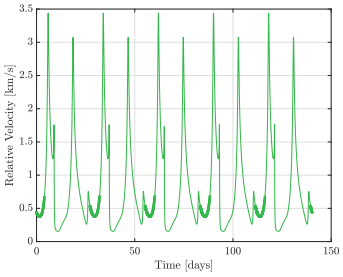

(e) Relative velocity.

Figure 11. Contour plot for total relay time for the observer in the 1:1 L_2 Lyapunov orbit. Data relay locations are highlighted in the Earth-Moon rotating frame.

significant for the locations at which the constellation spacecraft are within the nominal communications range of $120,000\ km$. For this analysis, the ideal relative phase determined previously for each observer is employed. The DRS and the observers are propagated for five months each; since the orbits are periodic, the behaviors over this time horizon reflect the general behavior that appears over longer times as well. The relative velocities for each observer are evaluated, with the locations at which each observer is within the nominal communications range of the DRS indicated via the bold arcs. For the observer in the L_1 Lyapunov orbit, the relative velocity during data relay lies between $170\ m/s$ and $530\ m/s$, as evident in the plot in Figure 9(e). For the observer in the 3:1 resonant orbit, Figure 10(e) illustrates the velocity with respect to the DRS in the 2:1 resonant orbit. At the relay locations, this velocity is bounded between $480\ m/s$ and $750\ m/s$, that coincides with apogee on the resonant orbit. Finally, for the L_2 Lyapunov observer, the relay velocity is between $375\ m/s$ and $680\ m/s$, as apparent in Figure 11(e).

Additional Surveillance Orbits

The process of selecting and evaluating the orbits in the surveillance constellation is extendable to other orbits as well. Additional observers that possess longer periods, such as observers in 4:3 resonant orbits, or orbits that go back and forth between the lunar near- and far-sides, such as members from the family of period-3 distant retrograde orbits (P3DROs) introduced in Figure 4(d), provide unique advantages that support surveillance needs.

In Figure 12, an assessment is summarized for surveillance via an observer in a P3DRO trajectory that is selected from the orbit family plotted in Figure 4(d). The selected orbit is characterized by a Jacobi constant value of 2.9964, and a period of $23.16\ days$. Although the orbit is not precisely resonant with the lunar sidereal period, due to its short $\hat{y}$-amplitude, it maintains a proximity with the Moon. The orbit geometry also allows the observer to shift back and forth between the far-side and near-side of the Moon, ballistically and without maneuvers. Thus, for tracking objects inside the surveillance cone, a space-based observer in this orbit is especially viable. Within the context of the previously defined surveillance constellation, the phasing for this observer relative to the data relay satellite is determined via the contour plot in Figure 12(a). Consistent with previous examples, the contour plot for the total relay time over one month reveals a non-intuitive relative phase with the DRS. Using the ideal phase difference between the two spacecraft, five-month trajectory baselines are constructed for the observer in the rotating frame and the inertial frame, as apparent in Figures 12(b) and 12(c), respectively. The bold arcs indicate the locations for data relays, with the DRS orbit - plotted in black. The observer is within communications range of the DRS for just under $22\ days$ over the 140-day propagation period, nearly 15% of the time. The relative velocity is plotted in Figure 12(e), and is bounded between $44\ m/s$ and $1.5\ km/s$ for the intervals when the DRS is within communications range. While the relay time is shorter than that of the observers in the previous examples, the orbit geometry is particularly useful and applicable for surveillance applications.

Surveillance via a longer-period sidereal resonant orbit, such as one from the 4:3 resonant orbit family in Figure 4(f), may be useful for the global monitoring of cislunar space. The Jacobi constant value for this orbit is equal to 2.9641, with a period of approximately $64.74\ days$. The longer period introduces challenges associated with the constellation phasing. However, leveraging the contour plot in Figure 13(a), the ideal phase is identified such that, over five months, the observer is within relay range for $36.87\ days$. In the rotating frame view in Figure 13(b), it is apparent that the observer in this orbit has opportunities for direct communications with the Earth as well. In the inertial frame

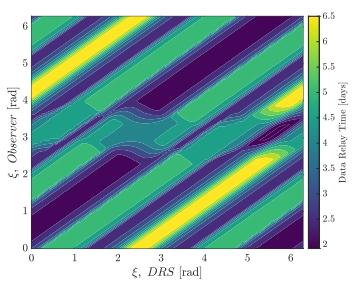

(a) Contour plot for total relay time.

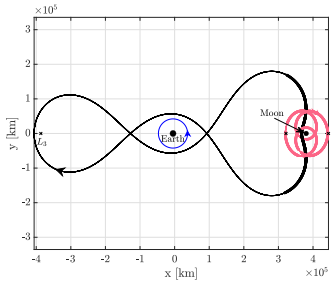

(b) Rotating frame view.

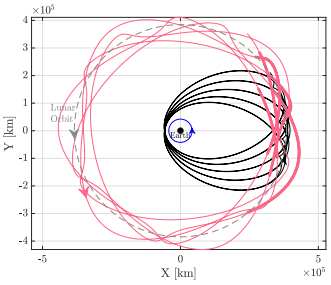

(c) Earth-centered inertial frame.

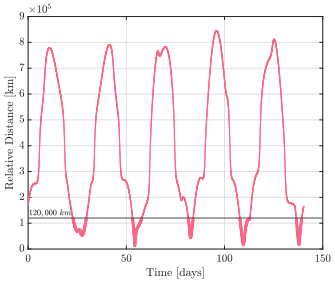

(d) Relative distance.

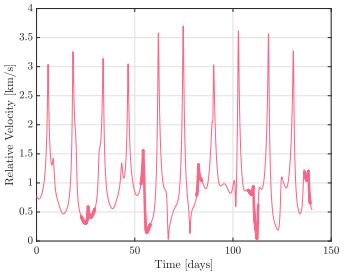

(e) Relative velocity.

Figure 12. Cislunar surveillance via a P3DRO observer over five months.

view in Figure 13(c), the surveillance advantages for this orbit are highlighted, demonstrating the larger areas swept by the orbit over the course of five months, with frequent Earth-Moon transfer opportunities as well.

EPHEMERIS VALIDATION OF CONSTELLATION ORBITS

Additional insight is gained by analyzing the constellation orbits in the N-body ephemeris model. In this investigation, a geometry-preserving transition process is employed to produce multi-revolution baselines in the ephemeris model for the DRS orbit and for each of the observer orbits. The transition approach employed in this investigation is adapted from the methodology detailed by Pavlak, and continuity in position and velocity is enforced in the ephemeris model via a differential corrections scheme.[17] Periodic orbits from the CR3BP transition into quasi-periodic trajectories in the ephemeris model that reflect the inherent CR3BP geometry. The trajectories are computed in a Sun-Earth-Moon-Jupiter ephemeris model, with the model epoch February 24, 2025, 00:00:00 UTC.[7]

The corrected ephemeris trajectories appear in Figure 14 for the 3:1 resonant orbit observer in purple, and the 2:1 resonant trajectory for the DRS in black. The trajectories are plotted in the J2000 Earth-centered inertial frame in Figure 14(b), also demonstrating the recurring Earth-Moon access via both orbits. Due to the stacking transition process, the trajectories generally retain their CR3BP geometries. Phasing between the orbits is also maintained to the same levels as observed in the CR3BP model. The trajectories are propagated for a total of $184\ days$; over this interval, the observer is within $120,000\ km$ of the DRS for approximately $22\ days$. The periodic interface between the observer and DRS is apparent in Figure 14(c). The relative velocities over the same time period are plotted in Figure 14(d), with the bold arcs highlighting the relay opportunities. For

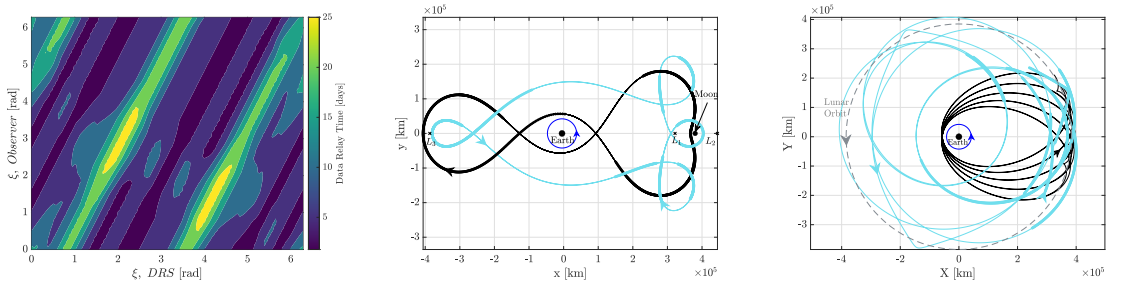

(a) Contour plot for total relay time. (b) Relay locations, rotating frame. (c) Relay locations, inertial frame.

(d) Relative distance. (e) Relative velocity.

Figure 13. Surveillance evaluation of a 4:3 resonant orbit observer over five months.

the observer in the L_1 Lyapunov orbit, a similar transition process yields the observer trajectory in Figures 15(a) and 15(b) in the rotating and inertial frames, respectively. The observer passes within nominal communications range for $49.6\ days$ of the 184-day time period. Consistent with previous examples, the relative phasing between the two spacecraft is maintained, due to the appropriately phased initial guess generated in the CR3BP model. The geometries are generally bounded as well, but may be refined to yield "tighter" trajectories if desired.

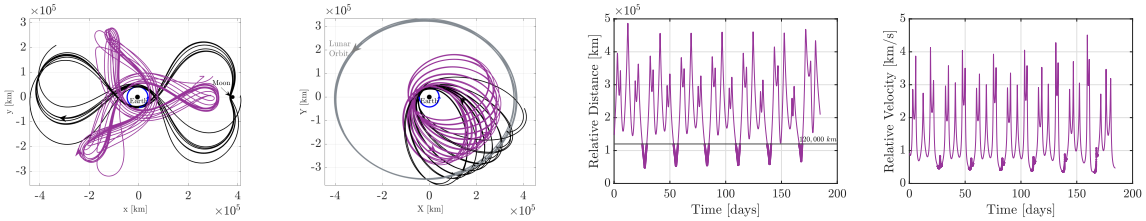

(a) Rotating frame. (b) J2000 inertial frame. (c) Relative distance. (d) Relative velocity.

Figure 14. Surveillance evaluation for a 3:1 resonant orbit observer in the Earth-Moon-Sun-Jupiter ephemeris model. Epoch: February 24, 2025, 00:00:00 UTC.

CONCLUDING REMARKS

Broad and localized surveillance of cislunar space presents challenges due to its large volume. As such, trajectories to support a multi-spacecraft constellation for space-based sensors are introduced in this investigation. Simultaneously, these observers are placed in various sidereal resonant orbits for overall surveillance and tracking and in libration point orbits for localized monitoring near the

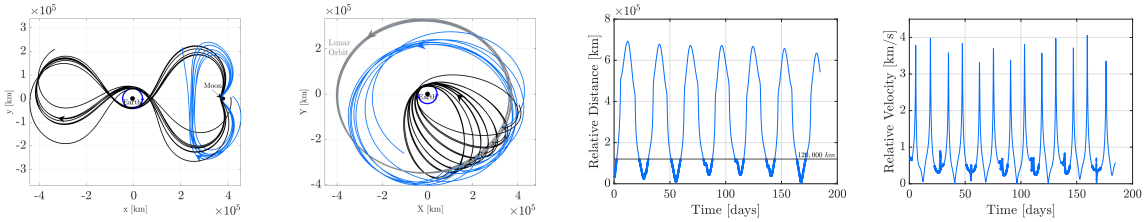

(a) Rotating frame. (b) J2000 inertial frame. (c) Relative distance. (d) Relative velocity.

Figure 15. Surveillance evaluation for a L_1 Lyapunov orbit observer in the Earth-Moon-Sun-Jupiter ephemeris model. Epoch: February 24, 2025, 00:00:00 UTC.

lunar vicinity. Another nontrivial aspect for surveillance trajectory design relates to communications with the Earth to relay surveillance data. In general, the observers do not necessarily remain in the proximity of the Earth. However, communications with the Earth are facilitated by the inclusion of a data relay satellite (DRS) in the surveillance constellation. The orbit of the DRS is selected such that it periodically approaches both the L_1-Moon-L_2 neighborhood and the vicinity of the geosynchronous orbit belt (GEO). Because of its proximity to these high-interest regions, inter-satellite communications between the DRS and the observers can aid data relay over long distances.

Various orbit options for hosting the observers are introduced. The surveillance and inter-satellite communications capabilities for spacecraft assumed to be operating in such orbits are summarized. Sidereal resonant orbits and libration point orbits in resonance with the Moon offer options for constellation orbits that maintain their relative configurations without maneuvers. To naturally maximize the opportunities for interfacing with the DRS in its orbit, a phasing strategy for the observers in their orbits is developed. A nominal value of $120,000\ km$ (selected arbitrarily) defines the maximum range within which the observer is assumed to be capable of relaying data to the DRS. This particular value is flexible and dependent on the spacecraft hardware. However, the process for selecting the relative phasing to increase the opportunities for data relay is applicable to other scenarios and specifications as well. For the orbits and the constellation architecture considered here, it is observed that placing the spacecraft at "apogee" maximizes the opportunities for data relay with the DRS assuming ballistic propagation in the CR3BP. While the maximum possible relay time over one month varies across the three observers, this preliminary analysis determines the phasing options that yield the most frequent opportunities for data relay for each observer.

Selecting orbits that are in equal sidereal resonances with the Moon, as well as each other, assists in maintaining the relative configuration of the constellation spacecraft. Independently, each observer collects surveillance data from the various regions of interest near the Moon and the libration points. Overall, the three-observer constellation, along with the data relay satellite, supplies surveillance capabilities in cislunar space. The observer in the 3:1 resonant orbit remains interior to the Earth-Moon system, naturally traversing back and forth between the L_1 libration point and the GEO belt. Supporting surveillance requirements beyond GEO, the remaining two observers in the Lyapunov orbits collect data from within the 30° surveillance cone. The orbits in the constellation are validated in the ephemeris model as well. The ballistic phasing and surveillance characteristics translate from the CR3BP into the ephemeris model. The process for evaluating the performance and feasibility of observer orbits introduced in the present work may be applied and extended to evaluate the performance of other periodic orbits in the CR3BP and, as the next step in fidelity, evaluate the constellation architecture in the ephemeris model as well. Additionally, the proposed

methodology is extendable to other orbits and varying number of observers and, thus, can be adapted for a long-term cislunar space domain awareness architecture.

ACKNOWLEDGEMENTS

The authors would like to thank the Purdue University School of Aeronautics and Astronautics for supporting this work. Valuable discussions with members of the Multi-Body Dynamics Research Group are also acknowledged. The authors also appreciate access to the computational facilities at the Barbara and Rune Eliasen Visualization Laboratory. Support is also appreciated under contract AFRL R1304009.

REFERENCES

[1] R. W. Farquhar, "The Utilization of Halo Orbits in Advanced Lunar Operations," *NASA X-551-70-449, Goddard Space Flight Center, Greenbelt, MD*, July 1971.

[2] S. Gao, W. Zhou, L. Zhang, W. Liang, D. Liu, and H. Zhang, "Trajectory design and flight results for Chang'e 4-relay satellite," *Zhongguo Kexue Jishu Kexue/Scientia Sinica Technologica*, 2019, 10.1360/N092018-00393.

[3] M. J. Volle, "Distant Retrograde Orbit Constellations for Relative-Only Navigation in Near Rectilinear Halo Orbits," July, 2022. https://ai-solutions.com/newsroom/about-us/news-multimedia/distant-retrograde-orbit-constellation/, last accessed at 2022-09-24.

[4] C. Frueh, K. Howell, K. DeMars, and S. Bhadauria, "Cislunar Space Situational Awareness," *31st AIAA/AAS Space Flight Mechanics Meeting*, Charlotte, North Carolina (Virtual), February, 2021.

[5] C. Frueh, K. Howell, K. DeMars, S. Bhadauria, and M. Gupta, "Cislunar Space Traffic Management: Surveillance through Earth-Moon Resonance Orbits," *8th European Conference on Space Debris*, Virtual, April, 2021.

[6] M. Gupta, K. C. Howell, and C. Frueh, "Earth-Moon Multi-Body Orbits to Facilitate Cislunar Surveillance Activities," *AAS/AIAA Astrodynamics Specialist Conference*, Big Sky, Montana (Virtual), August, 2021.

[7] M. Gupta, K. C. Howell, and C. Frueh, "Long-Term Cislunar Surveillance Via Multi-Body Resonant Trajectories," *AAS/AIAA Astrodynamics Specialist Conference*, Charlotte, North Carolina, August, 2022.

[8] "The Navigation and Ancillary Information Facility – SPICE Data (SPICE Kernels)," July, 2022. https://naif.jpl.nasa.gov/naif/data.html, last accessed at 2022-07-15.

[9] R. Broucke, *Periodic Orbits in the Restricted Three-Body Problem with Earth-Moon Masses*. California Institute of Technology, 1968. JPL Technical Report 82-1168.

[10] M. Vaquero, *Spacecraft Transfer Trajectory Design Exploiting Resonant Orbits in Multi-Body Environments*. Ph.D. Dissertation, Purdue University, West Lafayette, Indiana, 2013.

[11] R. L. Anderson, S. Campagnola, and G. Lantoine, "Broad Search for Unstable Resonant Orbits in the Planar Circular Restricted Three-Body Problem," *Celestial Mechanics and Dynamical Astronomy*, 2016, 10.1007/s10569-015-9659-7.

[12] E. Zimovan, "Characteristics and Design Strategies for Near Rectilinear Halo Orbits within the Earth-Moon System," M.S. Thesis, Purdue University, West Lafayette, Indiana, 2017.

[13] "Memorandum of Understanding between the National Aeronautics and Space Administration and the United States Space Force," September, 2020. https://www.nasa.gov/sites/default/files/atoms/files/nasa_ussf_mou_21_sep_20.pdf, last accessed at 2022-11-24.

[14] T. Hitchens, "AFRL Satellite To Track Up To The Moon; Space Force-NASA Tout Cooperation," September, 2020. https://breakingdefense.com/2020/09/afrl-satellite-to-track-up-to-the-moon-space-force-nasa-tout-cooperation/, last accessed at 2021-07-27.

[15] T. Hitchens, "Oracle's Vision: Understanding Cislunar Satellite Images Poses AFRL's 'Biggest' Challenge," November, 2022. https://breakingdefense.com/2022/11/oracles-vision-understanding-cislunar-satellite-images-poses-afrls-biggest-challenge/, last accessed at 2022-12-20.

[16] N. B. Lafarge, K. C. Howell, and D. C. Folta, "An Autonomous Stationkeeping Strategy for Multi-Body Orbits Leveraging Reinforcement Learning," *AIAA SciTech Forum*, San Diego, California, January, 2022.

[17] T. Pavlak, *Mission Design Applications in the Earth-Moon System: Transfer Trajectories and Stationkeeping*. M.S. Thesis, Purdue University, West Lafayette, Indiana, 2010.